ORIGINAL ARTICLE

Pulmonary Angiopathy in Severe COVID-19: Physiologic, Imaging, and Hematologic Observations

Brijesh V. Patel[1,2*], Deepa J. Arachchillage[3,4*], Carole A. Ridge[5,6*], Paolo Bianchi[7], James F. Doyle[7], Benjamin Garfield[7], Stephane Ledot[7], Cliff Morgan[7], Maurizio Passariello[7], Susanna Price[5,7], Suveer Singh[1,7], Louit Thakuria[7], Sarah Trenfield[7], Richard Trimlett[7], Christine Weaver[7], S. John Wort[5,8], Tina Xu[7], Simon P. G. Padley[5,6*], Anand Devaraj[5,6*], Sujal R. Desai[5,6*], and The Severe Acute Respiratory Failure Service and The Departments of Anaesthesia and Critical Care, Royal Brompton Hospital

[1]Division of Anaesthetics, Pain Medicine, and Intensive Care, Department of Surgery and Cancer, [3]Centre for Haematology, Department of Immunology and Inflammation, and [5]National Heart and Lung Institute, Imperial College London, London, United Kingdom; [2]Department of Adult Intensive Care, [4]Department of Haematology, [6]Department of Radiology, [7]Department of Adult Intensive Care, and [8]The Pulmonary Hypertension Service, Royal Brompton & Harefield NHS Foundation Trust, London, United Kingdom

ORCID IDs: 0000-0002-5573-2503 (B.V.P.); 0000-0001-5993-4850 (D.J.A.); 0000-0003-2510-5856 (C.A.R.); 0000-0001-9973-9283 (P.B.); 0000-0002-7060-0373 (J.F.D.); 0000-0001-9261-3186 (S.L.); 0000-0002-6425-3360 (S.P.); 0000-0003-3219-8966 (S.S.); 0000-0003-1298-6578 (L.T.); 0000-0002-7023-8044 (C.W.); 0000-0003-4287-1173 (S.J.W.); 0000-0002-7381-2339 (S.P.G.P.); 0000-0002-5237-3613 (S.R.D.).

Abstract

Rationale: Clinical and epidemiologic data in coronavirus disease (COVID-19) have accrued rapidly since the outbreak, but few address the underlying pathophysiology.

Objectives: To ascertain the physiologic, hematologic, and imaging basis of lung injury in severe COVID-19 pneumonia.

Methods: Clinical, physiologic, and laboratory data were collated. Radiologic (computed tomography (CT) pulmonary angiography [$n = 39$] and dual-energy CT [DECT, $n = 20$]) studies were evaluated: observers quantified CT patterns (including the extent of abnormal lung and the presence and extent of dilated peripheral vessels) and perfusion defects on DECT. Coagulation status was assessed using thromboelastography.

Measurements and Results: In 39 consecutive patients (male: female, 32:7; mean age, 53 ± 10 yr [range, 29–79 yr]; Black and minority ethnic, $n = 25$ [64%]), there was a significant vascular perfusion abnormality and increased physiologic dead space (dynamic compliance, 33.7 ± 14.7 ml/cm H_2O; Murray lung injury score, 3.14 ± 0.53; mean ventilatory ratios, 2.6 ± 0.8) with evidence of hypercoagulability and fibrinolytic "shutdown". The mean CT extent (±SD) of normally aerated lung, ground-glass opacification, and dense parenchymal opacification were 23.5 ± 16.7%, 36.3 ± 24.7%, and 42.7 ± 27.1%, respectively. Dilated peripheral vessels were present in 21/33 (63.6%) patients with at least two assessable lobes (including 10/21 [47.6%] with no evidence of acute pulmonary emboli). Perfusion defects on DECT (assessable in 18/20 [90%]) were present in all patients (wedge-shaped, $n = 3$; mottled, $n = 9$; mixed pattern, $n = 6$).

Conclusions: Physiologic, hematologic, and imaging data show not only the presence of a hypercoagulable phenotype in severe COVID-19 pneumonia but also markedly impaired pulmonary perfusion likely caused by pulmonary angiopathy and thrombosis.

Keywords: novel coronavirus disease 2019; acute respiratory distress syndrome; pulmonary perfusion; thoracic imaging; mechanical ventilation

(Received in original form April 27, 2020; accepted in final form July 14, 2020)

*These authors contributed equally to this work.

A list of members of the Severe Acute Respiratory Failure Service and the Departments of Anesthesia and Critical Care is provided in the online supplement.

Author Contributions: Study concepts and design: B.V.P., D.J.A., C.A.R., S.P.G.P., A.D., and S.R.D. Literature review: B.V.P., D.J.A., C.A.R., S.P.G.P., A.D., and S.R.D. Clinical data collection: all authors. Manuscript preparation/editing: B.V.P., D.J.A., C.A.R., S.P.G.P., A.D., and S.R.D. Data analysis: B.V.P., D.J.A., C.A.R., S.P.G.P., A.D., and S.R.D. Statistical analysis: B.V.P., C.A.R., and A.D. Final manuscript review: all authors.

Correspondence and requests for reprints should be addressed to Brijesh V. Patel, M.D., Ph.D., Division of Anaesthetics, Pain Medicine, and Intensive Care and Department of Surgery and Cancer, Faculty of Medicine, Imperial College London, and Department of Adult Intensive Care, The Royal Brompton and Harefield NHS Foundation Trust, Sydney Street, London SW3 6NP, UK. E-mail: brijesh.patel@imperial.ac.uk.

This article has a related editorial.

This article has an online supplement, which is accessible from this issue's table of contents at www.atsjournals.org.

Am J Respir Crit Care Med Vol 202, Iss 5, pp 690–699, Sep 1, 2020

Originally Published in Press as DOI: 10.1164/rccm.202004-1412OC on July 15, 2020
Internet address: www.atsjournals.org

At a Glance Commentary

Scientific Knowledge on the Subject: Accumulating data indicate that activation of inflammatory and coagulation pathways plays a major role in respiratory failure induced by coronavirus disease (COVID-19). Moreover, dysregulation of the pulmonary vasculature is believed to induce perfusion abnormalities and contribute to the physiological phenotypes reported in COVID-19 pneumonia.

What This Study Adds to the Field: Pulmonary vascular abnormalities including dilated peripheral vessels, the so-called "vascular tree-in-bud" pattern, and perfusion defects are common computed tomography findings in severe COVID-19 pneumonia. Physiologic observations and imaging studies, supported by point-of-care hematological assays, are important indicators of pulmonary angiopathy in COVID-19, potentially serving as a guide to disease severity and in monitoring progress.

The global spread of coronavirus disease (COVID-19), caused by severe acute respiratory syndrome coronavirus 2 (SARS-CoV-2), was classified a pandemic by the World Health Organization in March 2020. Respiratory failure is the dominant cause of death, and current management of COVID-19 centers on supportive care. However, it has been stated that respiratory physiology in COVID-19 differs from "conventional" acute respiratory distress syndrome (ARDS) (1). Emerging evidence suggests that aberrant and exuberant activation of inflammatory and coagulation cascades (termed "immunothrombosis") in COVID-19 pneumonia together with elevated levels of IL-6, D-dimer, lactate dehydrogenase (LDH), and ferritin on admission are linked with higher mortality (2–5).

The other major issue in COVID-19 is the fundamental role of endothelial injury and disrupted vasoregulation (6). Indeed, the latter has been proposed as a key component in early COVID-19–related ARDS (7). Accordingly, we examined a cohort of mechanically ventilated patients with severe COVID-19 pneumonia abnormalities focusing on *1*) physiologic data, *2*) findings on computed tomographic pulmonary angiography (CTPA), *3*) lung perfusion as demonstrated by dual-energy computed tomography (DECT) pulmonary blood volume "maps," and *4*) hematologic tests evidence of hypercoagulability and impaired fibrinolysis.

Methods

Study Design and Participants

This retrospective, observational study describes 39 consecutive mechanically ventilated patients with confirmed SARS-CoV-2 infection, admitted through a specialist severe respiratory failure and extracorporeal membrane oxygenation (ECMO) service. Patients were transferred from referral sites to our institution between March 17 and April 10, 2020. Eligible patients *1*) were laboratory-confirmed positive for COVID-19, *2*) were mechanically ventilated or on ECMO with active COVID-19–induced respiratory failure, and *3*) had undergone CTPA including, where feasible, DECT. All patients were transferred either for the possible requirement of ECMO support or for further management after having already been commenced on ECMO at the referring center.

The study was approved by the Research Ethics Committee (reference number: 20/EE/0160). All patients lacked capacity, and the need for individual informed consent was waived for retrospective analysis of data collected prospectively for routine care, with no breach of privacy or anonymity.

Data Collection

Demographic, clinical, laboratory, and treatment data were extracted from electronic medical records and a point-of-care testing database. Respiratory physiology measurements are presented as on admission and shortly before CT-scan imaging. All clinical data were reviewed and collated by investigating physicians (B.V.P. and D.J.A.).

Laboratory Procedures

SARS-CoV-2 infection was confirmed on real-time PCR assay. Routine blood examinations included *1*) complete blood count, *2*) coagulation profile, *3*) serum biochemical tests (including renal and liver function, LDH, and electrolytes), *4*) myocardial enzymes, and *5*) serum ferritin. Overall coagulation state and fibrinolysis were assessed using thromboelastography (TEG 6; Haemonetics) (*see* online supplement for interpretation). The frequency of investigations and further tests were determined by the treating physicians.

CT Image Acquisition and Interpretation

Full details regarding image acquisition protocols plus the quantification of morphologic CT patterns and perfusion defects on DECT images are provided in the online supplement. All patients were scanned in a dedicated COVID-19 CT suite using a second-generation dual-source CT system (Somatom Definition Flash; Siemens Healthineers). The methodology for CT interpretation was designed as an observational study, investigating a novel disease. Two observers (A.D. and S.R.D., both thoracic radiologists of 14 and 24 years' experience, respectively), reviewed all available CT studies by consensus, blinded to clinical data (*see* online supplement). In brief, the overall extent of abnormal lung (to the nearest 5%) and the percentage of aerated, ground-glass opacification, and dense parenchymal opacification (denoting consolidated and/or atelectatic lung), up to total of 100%, as a component of abnormal lung were visually quantified. Additionally, the presence of peripheral dilated (branching and tortuous) vessels in the lung not obscured by dense parenchymal opacification was recorded. The incidence of venous thrombosis was confirmed by review of reports of lower and upper limb compression ultrasound and/or CT venography where available. In 20 of 39 (51%) cases, CTPA studies were acquired using the DECT technique; in those, 18/20 had assessable lobes (*see* online supplement). Pulmonary blood volume images acquired using DECT were reviewed by two thoracic radiologists (C.R. and S.P.G.P.; 14 and 30 years' experience, respectively) (*see* online supplement) and evaluated for the presence/absence of perfusion defects and, when present, categorized as *1*) wedge-shaped, *2*) mottled, or *3*) mixed based on appearances described in chronic thromboembolic disease.

Statistical Analysis

Descriptive statistics were used to summarize the data; results are reported as medians and interquartile ranges or means and SD, as appropriate. Categorical variables were summarized as counts and percentages. Normality for continuous variables was tested with the D'Agostino and Pearson normality test. Two-tailed *t* test, Mann-Whitney *U* test, or Kruskal-Wallis test with Dunn's multicomparison was used to compare differences between groups where appropriate. Correlations were performed using Spearman correlation coefficient and nonlinear least squares regression fitting. A two-sided $P < 0.05$ was considered statistically significant. Statistical analyses were performed using GraphPad Prism v8.4 (GraphPad Software).

Results

Baseline Demographic and Clinical Characteristics of Patients with COVID-19

During the study period, 39 mechanically ventilated patients (male, 79.5%; mean age, 53 ± 10 yr; Black and minority ethnic, 64%) were admitted to our institution, of whom 20 (51%) also received ECMO support. The demographic and clinical characteristics are shown in Table 1. The mean duration of symptoms before hospital admission was 8.2 ± 3.5 days, and the mean time between hospital admission and endotracheal intubation was 1.3 ± 2.0 days. Comorbid chronic medical conditions and/or a body mass index >30 kg/m^2 were present in 80% of patients. Of the 20 patients on ECMO, 3 were placed onto ECMO at our center, having already been transferred, whereas 17 were transferred from referring ICUs on mobile ECMO. The mean number of days of mechanical ventilation at the referring center, prior to transfer, was 3.2 ± 3.1 days (range, 0–13 d). From admission, all patients received at least prophylactic dose of low-molecular-weight heparin or unfractionated heparin for patients on ECMO or renal replacement therapy.

Table 1. Clinical and Laboratory Characterization

Demographics and Clinical Characteristics	Number (%), Median (Range), or Mean (±SD)
Age	52.5 (29–79)
Sex, M	32 (82)
Sex, F	7 (18)
White	14 (36)
Black and minority ethnic	25 (64)
BMI, kg/m^2	31.3 (±6.1)
BMI > 30 kg/m^2	22 (57)
Diabetes mellitus	8 (21)
Hypertension	15 (39)
Asthma	3 (8)
Hyperlipidemia	2 (5)
Physiologic characteristics (on admission)	
Pa_{O_2}/FI_{O_2}	114.9 (±74.2)
Pa_{CO2}, mm Hg	63.6 (±20.6)
Minute ventilation, L/min	11.7 (±2.2)
Dynamic compliance, ml/cm H_2O	33.7 (±14.7)
Positive end-expiratory pressure, cm H_2O	12.3 (±2.4)
Murray lung injury score	3.14 (±0.53)
Ventilatory ratio	2.6 (±0.8)
Admission sequential organ failure score	8.0 (±2.5)
Admission APACHE II score	18.7 (±5.0)
Respiratory ECMO survival prediction score	3.4 (±1.9)
Laboratory tests on admission (normal values)	
White cell count, $\times 10^9$/L (3.6–11.0)	10.6 (±4.4)
Neutrophils, $\times 10^9$/L (1.8–7.5)	9.3 (±4.3)
Lymphocytes, $\times 10^9$/L (1.0–4.0)	0.76 (±0.4)
Creatinine, μmol/L (45–110)	172 (±141)
CRP, mg/L (<3)	305 (±101)
Ferritin, ng/ml (18–270)	987 (552–1,425)
Lactate dehydrogenase, U/L (<250)	996 (773–1,270)
Platelets, 10^9/L (146–360)	272 (±77)
Fibrinogen, g/L (1.5–4.5)	6.6 (±1.9)
Antithrombin 3, IU/dl (70–140)	70.6 (±23.7)
APTT, s (26–36)	38.8 (±13.1)
PT, s (10–12.5)	14.1 (±2.1)
D-dimer, ng/ml (208–318)	6,440 (±10,434)
High-sensitivity troponin, ng/L (<14)	143 (±262)
Brain natriuretic peptide, ng/L (<100)	186 (±274)

Definition of abbreviations: APACHE = The Acute Physiology and Chronic Health Evaluation; APTT = activated partial thromboplastin time; BMI = body mass index; CRP = C-reactive protein; ECMO = extracorporeal membrane oxygenation; PT = prothrombin time.

Physiologic and Laboratory Findings

The clinical and laboratory findings in all patients on admission are given in Table 1. Lymphocytopenia was a common finding with significantly elevated markers of organ damage and inflammation including creatinine, troponin, LDH, ferritin, and C-reactive protein. ARDS severity on admission was graded as moderate to severe: $Pa_{O_2}/FI_{O_2} = 114.9 \pm 74.2$ with dynamic respiratory system compliance (Crs) = 33.7 ± 14.7 ml/cm H_2O, and Murray lung injury score = 3.14 ± 0.53. Dynamic Crs was correlated with Pa_{O_2}/FI_{O_2} ($r = 0.49$; $P = 0.0017$). Increased positive end-expiratory pressure (PEEP) was associated with worse Pa_{O_2}/FI_{O_2} ($r = -0.38$; $P = 0.02$) and a higher ventilatory ratio (an indicator of ventilatory insufficiency and increased physiological dead space) ($r = 0.49$; $P = 0.0048$); furthermore, there was a strong negative correlation between Pa_{O_2}/FI_{O_2} and ventilatory ratio ($r = -0.65$; $P < 0.0001$) independent of dynamic Crs (Figure 1).

CTPA and DECT Findings

CTPA was performed in 39 patients, and, for reasons of technical limitation (i.e., body mass index ⩾35 or an inability to arm-raise), 20/39 (51%) underwent DECT. Eighteen of 39 (46%) patients were on ECMO at the time of CT; two patients were subsequently placed on ECMO and data were analyzed at the time of CT scan. The median interval between intubation and CT was 6 days (range, 0–18 d).

The mean CT extent of aeration, ground-glass opacification (%GGO), and

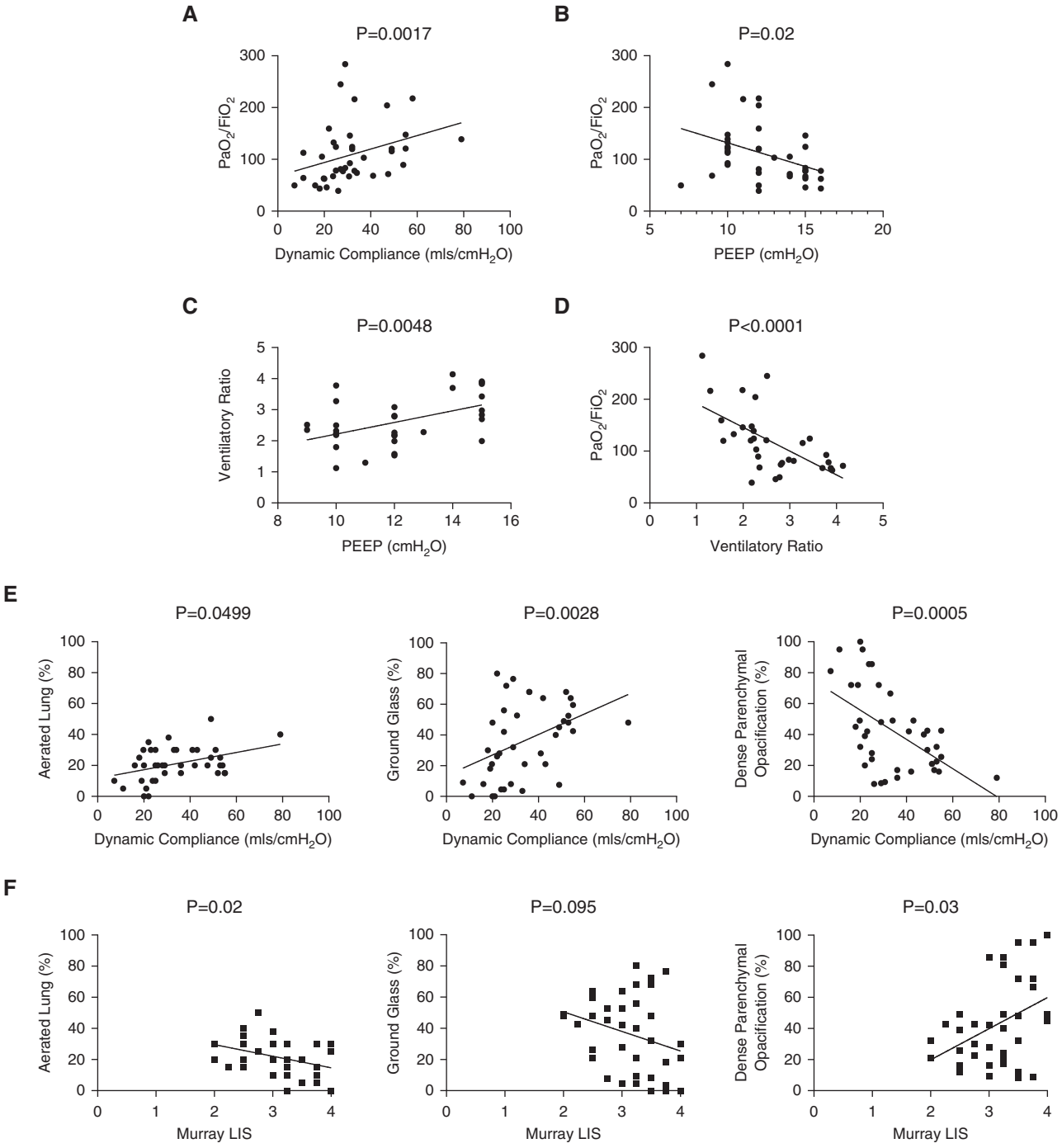

Figure 1. Physiologic correlations (on admission) between (*A*) Pa_{O_2}/Fi_{O_2} and dynamic respiratory system compliance ($N = 39$; $r = 0.485$; $P = 0.0017$); (*B*) $Pa_{O_2}/Fi_{O_2}$and positive end-expiratory pressure (PEEP) ($N = 38$; $r = -0.377$; $P = 0.02$); (*C*) ventilatory ratio (VR) and PEEP ($N = 32$; $r = 0.486$; $P = 0.0048$); (*D*) Pa_{O_2}/Fi_{O_2} and VR ($N = 38$; $r = -0.649$; $P < 0.0001$). (*E*) Associations between computed tomography (CT) features and dynamic compliance (on day of CT scan) showing positive correlations with percentage aeration ($N = 39$; $r = -0.316$; $P = 0.499$) and percentage ground-glass opacification ($N = 39$; $r = -0.466$; $P = 0.0028$) and negative correlations with dense parenchymal opacification ($N = 39$; $r = -0.362$; $P < 0.0001$). (*F*) Associations between CT features and Murray lung injury score showing negative correlations with percentage aeration ($N = 39$; $r = -0.365$; $P = 0.022$) and percentage ground-glass opacification ($N = 39$; $r = -0.271$; $P = 0.095$) and positive correlations with dense parenchymal opacification ($N = 39$; $r = 0.349$; $P = 0.03$). LIS = lung injury score.

dense parenchymal opacification (%DPO) were 21.1 ± 10.8%, 36.3 ± 24.7%, and 42.7 ± 27.1%, respectively (Table 1). Crs (on day of CT imaging) was positively correlated with extent of normally aerated lung ($P = 0.0499$) and %GGO ($P = 0.0028$) but negatively with the extent of %DPO ($P = 0.0005$) (Figure 1). There were no correlations between CT findings and Pa_{O_2}/Fi_{O_2} or ventilatory ratio.

There was a negative correlation in percentage aeration ($P = 0.02$) and positive

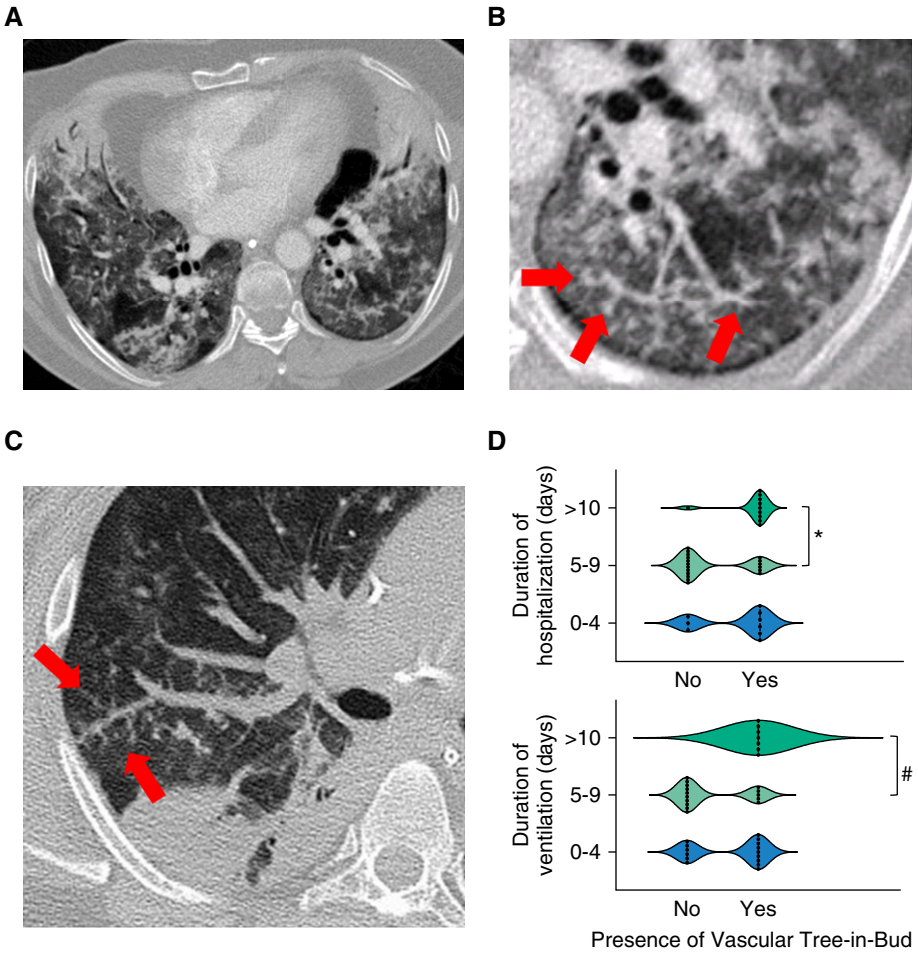

Figure 2. The computed tomography "vascular tree-in-bud pattern" in two patients with severe coronavirus disease (COVID-19) pneumonia. (*A*) A 52-year-old male patient scanned on day 1 following intubation. There is bilateral ground-glass opacification and patchy consolidation. Dilated branching and tortuous vessels are present in the left lower lobe representing the vascular tree-in-bud pattern. (*B*) Targeted, enlarged image of the left lower lobe in the same patient and from the same image slice showing bizarre dilated subsegmental vessels in greater detail (arrows). (*C*) Targeted image of the right lung in a second patient again showing striking dilatation of vessels in the right upper lobe and a vascular tree-in-bud pattern (arrows). (*D*) Relationship between the prevalence of the vascular tree-in-bud pattern and duration of hospitalization (*$P = 0.013$ with Kruskal-Wallis; Dunn's multicomparison $P = 0.0127$: group "5–9" vs. ">10") and ventilation (#$P = 0.0142$ with Kruskal-Wallis; Dunn's multicomparison $P = 0.0112$: group "5–9" vs. ">10").

correlation in %DPO ($P = 0.03$) with increasing severity of injury as assessed using the Murray lung injury score. There was tendency to reduction in %GGO with increasing with worsening injury (Figure 1).

Vascular Perfusion Abnormalities on CTPA and DECT Findings

Dilated (tortuous and branching) peripheral vessels (Figure 2) were present on CT in 21 out of 33 (63.6%) patients (Table 2) who had at least two "assessable" lobes (i.e., those with <50% obscuration by dense parenchymal opacification—*see* also online supplement); dilated peripheral vessels were seen in 10/21 (47.6%) without pulmonary embolism (PE). Arterial filling defects on CTPA, consistent with acute PE, were present in 15/39 (38%) patients. The prevalence of dilated peripheral vessels increased significantly with increasing duration of hospitalization and length of ventilation (Figure 2).

Lung parenchyma was considered assessable on DECT in 18/20 patients. Perfusion defects (Figure 3) were present in 18/18 (100%) patients, with a median extent of 46.3% (range, 20.0–77.5%) (Figure 3). Perfusion defects were classed as wedge-shaped (Videos E1A and E1B in the online supplement) in three patients, mottled (Videos E2A and E2B) in nine, and mixed (i.e., both wedge-shaped and mottled patterns coexisted; Videos E3A and E3Bb) in six (Figure 3). A healthy control DECT (Figure 3 and Video E4) shows a homogeneous color map indicating normal iodine distribution and perfusion.

Coagulation Abnormalities

D-dimer, platelet count, fibrinogen, prothrombin time, activated partial thromboplastin time, and antithrombin levels on admission are shown in Table 1. TEG data from the citrated kaolin heparinase channel showed hypercoagulability characterized by raised maximal amplitude (MA) and absent fibrinolysis (Figure 4A); the MA represents the maximal clot strength as determined by platelet number and function (of note, 80% of MA contribution is from platelets and the other 20% from fibrinogen). Twenty-one of 39 (54%) patients had MA above the normal reference range (52–69 mm) with an overall median MA of 69.2 mm (range, 52–75 mm) despite being on at least prophylactic dose of low-molecular-weight heparin or unfractionated heparin with factor Xa levels of 0.2–0.3 IU/ml. There were significantly raised functional fibrinogen levels in the citrated functional fibrinogen trace suggesting a strong contribution of platelets and fibrin to clot strength. Twenty-nine of 39 patients (74%) had functional fibrinogen levels higher than the normal reference range (15–32 mm) with an overall median of 56 mm (range, 23–69 mm). All patients showed absent fibrinolysis as evident by LY30 of 0% across the whole cohort, whereas normal fibrinolysis activation shows some evidence of activation by 30 minutes (Figure 4B).

Discussion

Mechanically ventilated patients with severe COVID-19 pneumonia present with hypercapnic respiratory failure (8) and a relatively preserved respiratory system compliance initially (9), reflecting increased pulmonary dead space and a predominant defect in pulmonary perfusion. To the best of our knowledge, the current study is the first to systematically evaluate the combined physiologic, hematologic, and

Table 2. Computed Tomography Abnormalities in 39 Mechanically Ventilated Patients with Severe COVID-19 Pneumonia

Computed Tomography Findings	All (*N* = *39*)	
Aerated lung, %	23.5 (±16.7)	
Ground-glass opacity, %	36.3 (±24.7)	
Dense parenchymal opacification, %	42.7 (±27.1)	
	Number of Patients	**Proportion (%)**
Pulmonary embolism	15	15/39 (38.5)
Dilated peripheral vessels	21	21/33* (63.6)
1–5 segments	14	14/21 (66.7)
6–10 segments	7	7/21(33.3)
>10 segments	0	0/21 (0)
Dilated peripheral vessels without PE	10	10/21 (47.6)
Perfusion defect present	18	18/18† (100)
1–5 segments	14	14/18 (77.8)
6–10 segments	4	4/18 (22.2)
>10 segments	0	0/18
Perfusion defects without PE	8	8/18 (44.4)
DECT perfusion defect morphology		
Wedge shaped	3	3/18 (16.7)
Mottled	9	9/18 (50)
Mixed pattern	6	6/18 (33.3)
Deep venous thrombosis	4	4/22‡ (18.2)

Definition of abbreviations: COVID-19 = coronavirus disease; DECT = dual-energy computed tomography; PE = pulmonary embolism.
*Of 39 patients, 33 had at least two assessable lobes not obscured by dense collapse or consolidation.
†Of 20 patients, 18 had at least two assessable lobes on pulmonary blood volume color maps.
‡Twenty-two patients underwent peripheral limb ultrasound or computed tomography venography.

morphologic abnormalities in patients with COVID-19 pneumonia. Our observations point to an increased physiologic dead space, hypercoagulability (with absent fibrinolysis), and imaging signs of major vascular involvement. Accordingly, and in light of emerging pathologic evidence of major vascular involvement (6, 10, 11), we suggest that our results support the presence of a widespread pulmonary angiopathy in severe COVID-19 pneumonia.

Interest in the physiology of COVID-19–induced ARDS stemmed from the proposal by Gattinoni and colleagues of two broad (but almost certainly overlapping) phenotypes: "type L," with high lung compliance and limited ground-glass opacification on CT and responsive to lower PEEP, and "type H," in which compliance is low and disease more extensive on CT, potentially benefitting from higher PEEP (1). This apparently simple dichotomy has attractions but has been questioned: Bos and colleagues found no relationship between compliance and qualitative CT measurements, suggesting that these phenotypes may not be mutually exclusive (12). However, our data also confirm considerable overlap in phenotypes, with all patients showing a significant (>50% of lung volume) combination of ground-glass and diffuse parenchymal opacification, presumably related to the progression of disease. The latter was confirmed with patients showing a higher Murray lung injury score showing lower percentage aeration/ground-glass opacification but greater dense parenchymal opacification.

The ventilatory ratio—a simple bedside index of physiological dead space fraction in patients with ARDS (13)—was associated with worsening hypoxemia, in line with other studies of COVID-19–related ARDS (14). Moreover, the association between higher PEEP (i.e., lower Pa_{O_2}/Fi_{O_2}) and worsening hypoxemia and greater physiological dead space fraction (i.e., higher ventilatory ratio) all point to disproportionate vascular dysregulation compounded by redirection of perfusion away from overdistended oxygenated alveoli, without the benefits of additional lung recruitment, in line with recent studies of the variable efficacy of lung recruitment in COVID-19–induced ARDS (15, 16).

Two crucial observations from our study shed light on the possible pathophysiological explanation for this increased physiological dead space: first, the frequent presence of dilated, branching, and/or tortuous vessels in the peripheral lung, and second, perfusion defects on DECT. We believe that the dilatation of peripheral vessels is an extension of the enlarged vessels reported by others (17–19). Albarello and colleagues commented on enlarged tubular vessels in two patients (17). In a larger study, Caruso and coworkers found enlarged subsegmental vessels in 89% of 158 patients (19). The peripheral location and branching nature of the dilated vessels in our study bears a striking resemblance to the CT findings in rare patients with pulmonary tumor thrombotic microangiopathy (20): in the first report of its kind, the authors described the pathologic and CT features of a 48-year-old patient with progressive breathlessness. On thin-section CT, there were bilateral longitudinal branching opacities, the so-called "vascular tree-in-bud" pattern. Cardiac catheterization confirmed severe pulmonary hypertension, and at postmortem, most small arteries and arterioles were occluded by fibrocellular intimal hyperplasia and clumps of tumor cells were seen in some arterioles. The logical explanation, presumably, is that the small arterioles—normally *not* resolved on CT—were enlarged and thus rendered visible (20). It has been previously suggested that vessel enlargement in COVID-19 pneumonia might be a marker of increased blood flow (21). However, we do not subscribe to this explanation but instead suspect that the vascular tree-in-bud pattern in COVID-19 likely is a manifestation of pulmonary thrombotic angiopathy. Support for this comes from postmortem data (11, 22). In one of these studies, features of diffuse alveolar damage were present in all cases, but COVID-19 lungs were distinguished by the presence of widespread microthromboses and striking new vessel growth; the latter was termed "intussusceptive angiogenesis" and linked with increasing hospitalization (11). Intriguingly, albeit in a small number, we also found a linkage between the vascular tree-in-bud pattern and duration of both hospitalization and ventilation before CT. Thus, it is tempting to speculate that the

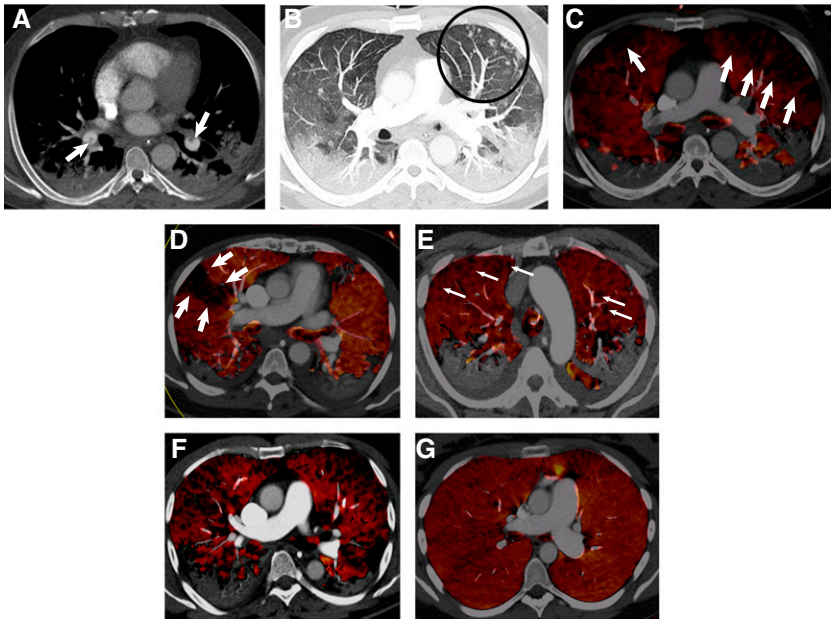

Figure 3. (*A–C*) Computed tomography (CT) pulmonary angiography and dual-energy CT (DECT) perfusion in a 47-year-old male patient with coronavirus disease (COVID-19) pneumonia, day 9 after intubation. (*A*) Soft-tissue reconstruction showing filling defects in lower lobe pulmonary arteries (thick arrows). (*B*) Maximal-intensity-projection CT images showing vascular tree-in-bud pattern (circled) in the left upper lobe anterolaterally and (*C*) corresponding DECT perfused blood volume color map showing widespread perfusion defects (thick arrows). (*D–F*) Representative DECT perfused blood volume color maps in three patients showing wedge-shaped (thick arrows) (*D*), mottled (thin arrows) (*E*), and mixed (*F*) perfusion defects. (*G*) Axial perfused blood volume images of the lungs in a 32-year-old female patient without COVID-19 or pulmonary embolism demonstrates a homogeneous color map indicating normal iodine distribution.

vascular tree-in-bud pattern in COVID-19 pneumonia may be an important CT marker of immunothrombosis and angiogenesis.

The DECT scanning technique, although lacking a *routine* role in the imaging of lung disease, has certainly attracted attention as an alternative means of assessing pulmonary perfusion in acute and chronic thromboembolic disease (23–25). In the specific context of chronic thromboembolic disease, there is high concordance between findings on DECT and traditional ventilation-perfusion imaging (24, 25). Indeed, patterns of perfusion abnormality appear to differ significantly between chronic thromboembolic disease and patients with pulmonary arterial hypertension (24). The striking finding of abnormal pulmonary perfusion on DECT has not, to the best of our knowledge, been fully explored in COVID-19 pneumonia (21). Abnormalities of perfusion were seen in all patients with assessable lobes, irrespective of whether this was in dependent or nondependent areas of the lung. This finding in patients with the most severe COVID-19–related respiratory failure suggests that vascular dysregulation is not, as has been proposed, restricted to those with the early or so-called "type L" phenotype (7). The finding of abnormal perfusion, although supporting the hypothesis of major vascular involvement, was certainly unexpected in the context of ARDS where, given the inflammatory pathology, one might have expected regions of overperfused lung on DECT (26).

Given the preferential respiratory route of entry and significant expression of ACEII in vascular endothelium (27), it might be speculated that SARS-CoV-2 might, through direct endothelial infection (facilitated by the ACEII receptor uptake), lead to significant pulmonary microvascular endothelial injury with associated viremia (6). Interestingly, SARS-CoV-1 has been shown to induce pulmonary cellular necrosis (28), and the pathobiological processes leading to immunothrombosis (endothelial injury, vascular inflammation, and thrombotic microangiopathy) might then serve to explain our observation of dilated peripheral vessels and perfusion defects on imaging. Furthermore, the vascular injury and so-called "cytokine storm" of COVID-19, with its release of eicosanoids (e.g., arachidonic acid), could stimulate platelet aggregation, simultaneous with a release of adenine nucleotides from activated platelets promoting thrombus formation, further amplifying the platelet response (29, 30). Indeed, pulmonary vascular inflammation, in particular, leukocyte–platelet interactions, is associated with the development of ARDS from non-COVID etiologies (31).

The issue of deep venous thrombosis (DVT) and acute PE in COVID-19 pneumonia merits brief consideration. Approximately 90% of symptomatic PEs are known to originate from thrombi located in lower limbs (32, 33). Moreover, in line with other viral pneumonias (34, 35), PE is reported in patients with COVID-19 (36, 37) and, admittedly, was present on CT in 15 of 39 patients in our study. Thus, it might conceivably be argued that the dilated peripheral vessels in our patients were simply being rendered visible on CT by embolic material from upper- or lower-limb DVT. However, against this, DVT was recorded in only 4 of 22 patients undergoing lower-limb compression ultrasound or CT venography, and only 1 patient with PE had DVT. Furthermore, it is noteworthy that dilatation of peripheral vessels with embolic material has, as far as we are aware, never been documented in patients with acute or chronic PE. Although accepting fully that DVT occurs commonly in critically ill patients (and that these may result in PE), we suggest that in COVID-19 there may be dual pathologies at play, namely, acute PE from DVT and a widespread pulmonary angiopathy.

We regard the hematological tests in our patients as important and complementary, serving to confirm hypercoagulability (as evidenced by raised MA, functional fibrinogen levels), and absent fibrinolysis given the LY30 of 0% in all patients. The term fibrinolysis "shutdown" refers to the acute impairment of fibrinolysis (38). Impaired fibrinolysis is regarded as a predictor of first and recurrent PE (39). Although use of TEG outside cardiac surgery and liver disease is limited, there is emerging evidence from several studies for a role for viscoelastic tests in assessing the bleeding and thrombotic risk in critically ill patients with infection/inflammation (40). Furthermore, hypercoagulability as

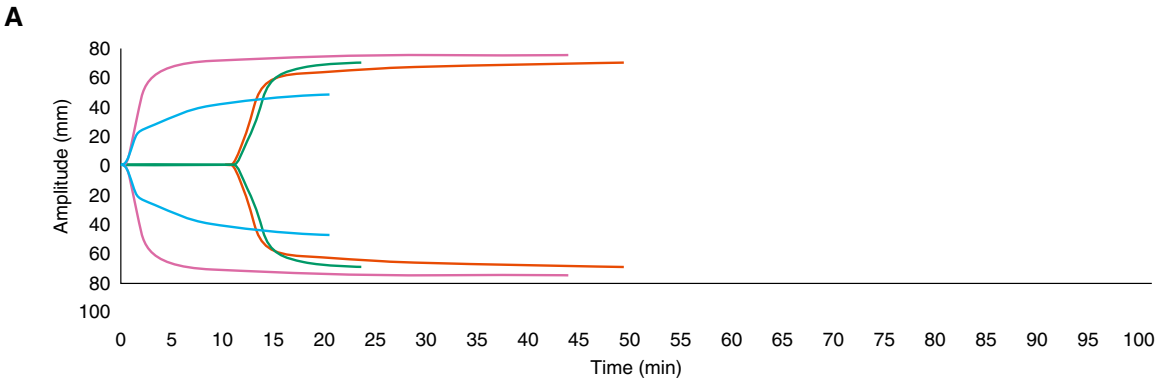

	TEG–ACT (sec)	R (min)	K (min)	ANGLE (deg)	A10 (mm)	MA (mm)	LY30 (%)
CK		11.0	1.2	77.5		62.7	0.0
		4.6 – 9.1	0.8 – 2.1	63 – 78		52 – 69	0..0 – 2.6
CRT	106.6	0.6	0.7	81.6	72.4	73.4	0.0
	82 –152	0.3 –1.1	0.8 –2.7	60 –78	44 –67	52 – 70	0.0 – 2.2
CKH		11.3	1.3	75.7		70.6	
		4.3 – 8.3	0.8 – 1.9	64 – 77		52.69	
CFF					43.2	48.5	
					15 – 30	15 – 32	

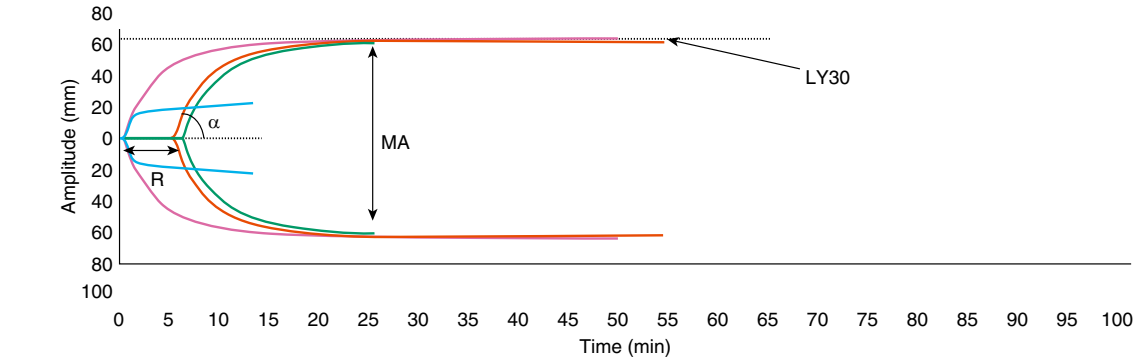

	TEG–ACT (sec)	R (min)	K (min)	ANGLE (deg)	A10 (mm)	MA (mm)	LY30 (%)
CK		5.4	1.1	74.5		62.6	0.1
		4.6 – 9.1	0.8 – 2.1	63 – 78		52 – 69	0.0 – 2.6
CRT	97.3	0.5	1.0	77.0	58. 1	63.1	0.0
	82 – 152	0.3 – 1.1	0.8 – 2.7	60 – 78	44 – 67	52 – 70	0.0 – 2.2
CKH		6.2	1.2	73.3		61.5	
		4.3 – 8.3	0.8 – 1.9	64 – 77		52 – 69	
CFF					22.2	23.0	
					15 – 30	15 – 32	

Figure 4. Representative thromboelastography (TEG) tracings of a (*A*) ventilated patient with coronavirus disease (COVID-19) and (*B*) a control healthy volunteer. The patient TEG shows universal hypercoagulability, with higher α-angle and maximal amplitude (MA), and absent fibrinolysis at 30 minutes (LY30 = 0%). The most frequently used parameters in TEG include reaction time, which reflects the time of latency from start of test to initial fibrin formation, which is prolonged if the patient is on an anticoagulant or has a coagulation factor deficiency. Heparinase TEG eliminates the effect of heparin. The α-angle measures the speed at which fibrin buildup and cross-linking takes place and hence assesses the rate of clot formation but also provides information on fibrin formation and cross-linking. The MA is a measure of the ultimate strength of the fibrin clot, that is, the overall stability of the clot. This is dependent on platelets (80%) and fibrin (20%) interactions. Fibrinolysis activation (the percentage lysis at 30 min after MA) is evident in the control TEG with the red trace beginning to decrease in amplitude. In contrast, the COVID-19 red trace continues to show a slow increase in amplitude. A10 = amplitude 10 minutes after the time blood starts to clot; ACT = activated clotting time; CFF = citrated blood sample activated by the functional fibrinogen test; CK = citrated blood sample activated with kaolin; CKH = citrated blood sample activated with kaolin and heparinase; CRT = citrated blood sample activated with RapidTEG; K = coagulation time (min); LY30 = percentage lysis at 30 minutes after MA; R = reaction time.

evidence by TEG has been shown to be predictive of thrombosis in patients with trauma and in the general population (41).

There are clear limitations to our study, not least the small sample size, the retrospective observational nature, the absence of matched (non–COVID-19) controls, the lack of a validation cohort, and, given the tertiary nature of our practice, the focus on patients with severe COVID-19–induced respiratory failure. The physiology does not directly prove pulmonary angiopathy, but we believe such relatively simple bedside physiological assessments may enable further diagnostic evaluation of vascular abnormalities and pulmonary angiopathy in severe COVID-19. Future studies comparing a matched control group of patients with non–COVID-19–related ARDS are clearly necessary to ascertain whether the imaging findings we report herein are truly related to SARS-CoV-2. However, in light of current evidence of a significant vascular component to COVID-19 (7, 11), we propose that our observations not only provide important noninvasive evidence of pulmonary vascular involvement through imaging but also add to the understanding of clinicophysiological phenotypes and pathobiology of COVID-19 pneumonia/ARDS.

In summary, our observations on CTPA and DECT, coupled with the physiologic and hematologic features, point to major pulmonary vascular involvement in severe COVID-19 pneumonia. Further validation of these imaging markers is clearly warranted, but in light of the emerging pathologic evidence of angiopathy, we believe our findings have implications for further pathobiologic and therapeutic studies. ■

Author disclosures are available with the text of this article at www.atsjournals.org.

References

1. Gattinoni L, Coppola S, Cressoni M, Busana M, Rossi S, Chiumello D. COVID-19 does not lead to a "typical" acute respiratory distress syndrome. *Am J Respir Crit Care Med* 2020;201:1299–1300.
2. Ruan Q, Yang K, Wang W, Jiang L, Song J. Clinical predictors of mortality due to COVID-19 based on an analysis of data of 150 patients from Wuhan, China. *Intensive Care Med* 2020;46:846–848.
3. Chen G, Wu D, Guo W, Cao Y, Huang D, Wang H, *et al*. Clinical and immunological features of severe and moderate coronavirus disease 2019. *J Clin Invest* 2020;130:2620–2629.
4. Tang N, Li D, Wang X, Sun Z. Abnormal coagulation parameters are associated with poor prognosis in patients with novel coronavirus pneumonia. *J Thromb Haemost* 2020;18:844–847.
5. Klok FA, Kruip MJHA, van der Meer NJM, Arbous MS, Gommers DAMPJ, Kant KM, *et al*. Incidence of thrombotic complications in critically ill ICU patients with COVID-19. *Thromb Res* 2020;191:145–147.
6. Varga Z, Flammer AJ, Steiger P, Haberecker M, Andermatt R, Zinkernagel AS, *et al*. Endothelial cell infection and endotheliitis in COVID-19. *Lancet* 2020;395:1417–1418.
7. Marini JJ, Gattinoni L. Management of COVID-19 respiratory distress. *JAMA* [online ahead of print] 24 Apr 2020; DOI: 10.1001/jama.2020.6825.
8. Liu X, Liu X, Xu Y, Xu Z, Huang Y, Chen S, *et al*. Ventilatory ratio in hypercapnic mechanically ventilated patients with COVID-19-associated acute respiratory distress syndrome. *Am J Respir Crit Care Med* 2020;201:1297–1299.
9. Bhatraju PK, Ghassemieh BJ, Nichols M, Kim R, Jerome KR, Nalla AK, *et al*. Covid-19 in critically ill patients in the Seattle region - case series. *N Engl J Med* 2020;382:2012–2022.
10. Fox SE, Akmatbekov A, Harbert JL, Li G, Quincy Brown J, Vander Heide RS. Pulmonary and cardiac pathology in African American patients with COVID-19: an autopsy series from New Orleans. *Lancet Respir Med* [online ahead of print] 27 May 2020; DOI: 10.1016/S2213-2600(20)30243-5.
11. Ackermann M, Verleden SE, Kuehnel M, Haverich A, Welte T, Laenger F, *et al*. Pulmonary vascular endothelialitis, thrombosis, and angiogenesis in Covid-19. *N Engl J Med* [online ahead of print] 21 May 2020; DOI: 10.1056/NEJMoa2015432.
12. Bos LD, Paulus F, Vlaar APJ, Beenen LFM, Schultz MJ. Subphenotyping acute respiratory distress syndrome in patients with COVID-19: consequences for ventilator management. *Ann Am Thorac Soc* 2020;17:1162–1164.
13. Sinha P, Calfee CS, Beitler JR, Soni N, Ho K, Matthay MA, *et al*. Physiologic analysis and clinical performance of the ventilatory ratio in acute respiratory distress syndrome. *Am J Respir Crit Care Med* 2019;199:333–341.
14. Liu X, Liu X, Xu Y, Xu Z, Huang Y, Chen S, *et al*. Ventilatory ratio in hypercapnic mechanically ventilated patients with COVID-19-associated acute respiratory distress syndrome. *Am J Respir Crit Care Med* 2020;201:1297–1299.
15. Haudebourg A-F, Perier F, Tuffet S, de Prost N, Razazi K, Mekontso Dessap A, *et al*. Respiratory mechanics of COVID-19– versus non–COVID-19–associated acute respiratory distress syndrome. *Am J Respir Crit Care Med* 2020;202:287–290.
16. Pan C, Chen L, Lu C, Zhang W, Xia JA, Sklar MC, *et al*. Lung recruitability in COVID-19-associated acute respiratory distress syndrome: a single-center observational study. *Am J Respir Crit Care Med* 2020;201:1294–1297.
17. Albarello F, Pianura E, Di Stefano F, Cristofaro M, Petrone A, Marchioni L, *et al*.; COVID 19 INMI Study Group. 2019-novel coronavirus severe adult respiratory distress syndrome in two cases in Italy: an uncommon radiological presentation. *Int J Infect Dis* 2020;93:192–197.
18. Bai HX, Hsieh B, Xiong Z, Halsey K, Choi JW, Tran TML, *et al*. Performance of radiologists in differentiating COVID-19 from viral pneumonia on chest CT. *Radiology* [online ahead of print] 10 Mar 2020; DOI: 10.1148/radiol.2020200823.
19. Caruso D, Zerunian M, Polici M, Pucciarelli F, Polidori T, Rucci C, *et al*. Chest CT features of COVID-19 in Rome, Italy. *Radiology* [online ahead of print] 3 Apr 2020; DOI: 10.1148/radiol.2020201237.
20. Franquet T, Giménez A, Prats R, Rodríguez-Arias JM, Rodríguez C. Thrombotic microangiopathy of pulmonary tumors: a vascular cause of tree-in-bud pattern on CT. *AJR Am J Roentgenol* 2002;179: 897–899.
21. Oudkerk M, Büller HR, Kuijpers D, van Es N, Oudkerk SF, McLoud TC, *et al*. Diagnosis, prevention, and treatment of thromboembolic complications in COVID-19: report of the National Institute for Public Health of the Netherlands. *Radiology* [online ahead of print] 23 Apr 2020; DOI: 10.1148/radiol.2020201629.
22. Fox SE, Akmatbekov A, Harbert JL, Li G, Brown JQ, Vander Heide RS. Pulmonary and cardiac pathology in African American patients with COVID-19: an autopsy series from New Orleans. *Lancet* 2020;8: 681–686.
23. Remy-Jardin M, Faivre JB, Pontana F, Molinari F, Tacelli N, Remy J. Thoracic applications of dual energy. *Semin Respir Crit Care Med* 2014;35:64–73.
24. Giordano J, Khung S, Duhamel A, Hossein-Foucher C, Bellèvre D, Lamblin N, *et al*. Lung perfusion characteristics in pulmonary arterial hypertension (PAH) and peripheral forms of chronic thromboembolic pulmonary hypertension (pCTEPH): dual-energy CT experience in 31 patients. *Eur Radiol* 2017;27:1631–1639.
25. Masy M, Giordano J, Petyt G, Hossein-Foucher C, Duhamel A, Kyheng M, *et al*. Dual-energy CT (DECT) lung perfusion in pulmonary hypertension: concordance rate with V/Q scintigraphy in diagnosing chronic thromboembolic pulmonary hypertension (CTEPH). *Eur Radiol* 2018;28:5100–5110.
26. Takeuchi H, Suzuki S, Machida H, Ishikawa T, Ueno E. Preliminary results: can dual-energy computed tomography help distinguish cardiogenic pulmonary edema and acute interstitial lung disease? *J Comput Assist Tomogr* 2018;42:39–44.

27. Hamming I, Timens W, Bulthuis ML, Lely AT, Navis G, van Goor H. Tissue distribution of ACE2 protein, the functional receptor for SARS coronavirus: a first step in understanding SARS pathogenesis. *J Pathol* 2004;203:631–637.
28. Yue Y, Nabar NR, Shi CS, Kamenyeva O, Xiao X, Hwang IY, *et al*. SARS-coronavirus open reading Frame-3a drives multimodal necrotic cell death. *Cell Death Dis* 2018;9:904.
29. Engelmann B, Massberg S. Thrombosis as an intravascular effector of innate immunity. *Nat Rev Immunol* 2013;13:34–45.
30. Dennis EA, Norris PC. Eicosanoid storm in infection and inflammation. *Nat Rev Immunol* 2015;15:511–523.
31. Abdulnour RE, Gunderson T, Barkas I, Timmons JY, Barnig C, Gong M, *et al*. Early intravascular events are associated with development of acute respiratory distress syndrome: a substudy of the LIPS-A clinical trial. *Am J Respir Crit Care Med* 2018;197:1575–1585.
32. Hyers TM. Venous thromboembolism. *Am J Respir Crit Care Med* 1999; 159:1–14.
33. Kearon C. Natural history of venous thromboembolism. *Circulation* 2003;107(Suppl 1):I22–I30.
34. Bunce PE, High SM, Nadjafi M, Stanley K, Liles WC, Christian MD. Pandemic H1N1 influenza infection and vascular thrombosis. *Clin Infect Dis* 2011;52:e14–e17.
35. Ishiguro T, Matsuo K, Fujii S, Takayanagi N. Acute thrombotic vascular events complicating influenza-associated pneumonia. *Respir Med Case Rep* 2019;28:100884.
36. Danzi GB, Loffi M, Galeazzi G, Gherbesi E. Acute pulmonary embolism and COVID-19 pneumonia: a random association? *Eur Heart J* 2020;41:1858.
37. Xie Y, Wang X, Yang P, Zhang S. COVID-19 complicated by acute pulmonary embolism. *Radiol Cardiothorac Imaging* 2020;2:e200067.
38. Moore HB, Moore EE, Liras IN, Gonzalez E, Harvin JA, Holcomb JB, *et al*. Acute fibrinolysis shutdown after injury occurs frequently and increases mortality: a multicenter evaluation of 2,540 severely injured patients. *J Am Coll Surg* 2016;222:347–355.
39. Morris TA, Marsh JJ, Chiles PG, Auger WR, Fedullo PF, Woods VL Jr. Fibrin derived from patients with chronic thromboembolic pulmonary hypertension is resistant to lysis. *Am J Respir Crit Care Med* 2006; 173:1270–1275.
40. Haase N, Ostrowski SR, Wetterslev J, Lange T, Møller MH, Tousi H, *et al*. Thromboelastography in patients with severe sepsis: a prospective cohort study. *Intensive Care Med* 2015;41:77–85.
41. Brill JB, Badiee J, Zander AL, Wallace JD, Lewis PR, Sise MJ, *et al*. The rate of deep vein thrombosis doubles in trauma patients with hypercoagulable thromboelastography. *J Trauma Acute Care Surg* 2017;83:413–419.